ELECTRONIC SUPPLEMENTARY INFORMATION

Solvent-dependent on/off valving using selectively permeable barriers in paper microfluidics

G. IJ. Salentijn,[a,b] N. N. Hamidon[a] and E. Verpoorte[a,†]

[a] Pharmaceutical Analysis, Groningen Research Institute of Pharmacy, University of Groningen, THE NETHERLANDS
[b] TI-COAST, Science Park 904, 1098 XH Amsterdam, THE NETHERLANDS
[†] Corresponding author

Table of contents:

Table S-1: Printing, slicing and miscellaneous parameters for 3D-printed mask (PLA, Arnitel) and clamp (ABS) parts for the first AKD patterning step.

Process	Parameter	PLA	Arnitel	ABS
Slicing	Resolution	0.13 mm (z) / 0.26 mm (xy)	0.13 mm (z) / 0.26 mm (xy)	0.2 mm (z) / 0.38 mm (xy)
	Infill solidity[a]	6	6	0.2
	Infill pattern	n/a	n/a	Grid hexagonal
	Shell nr.[b]	1	1	3
Printing	Filament flow[c]	100%	100%	100%
	Printing speed[d]	100%	60%	200%
	Extruder temp.	200 ^{O}C	200 ^{O}C	230 ^{O}C
	Print bed temp.	60 ^{O}C	60 ^{O}C	80 ^{O}C
Misc.		n/a	Printed on top of PLA layers	Printed on top of PLA layers, which are taped to the plate

[a] Ratio between the volume occupied by 3D-printed material and by air in the internal regions of a printed part

[b] Number of adjacent threads of 3D-printed material defining the contours of a printed structure

[c] Scaled to the printing speed. An increase in this number, means a higher flow of filament relative to the printing speed, which leads to thicker filament threads. Filament flow can be varied between 50% and 150% in the printing software.

[d] For all parts, the main printing speed was set to 70 mm/s in the slicing software. Structures like the first layer and shells are generally programmed at lower printing speed in the slicing software. The printing speed can be adjusted between 25% and 300% (of 70 mm/s) in the printing software.
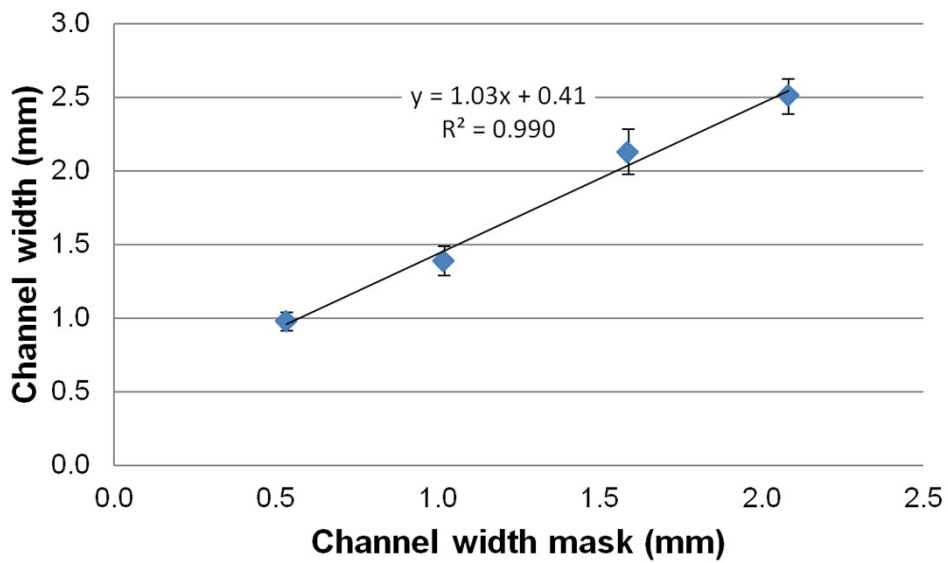
Figure S-1: Characterization of the paper patterns with water/methanol 1:3 (v/v) after the second AKD application step. The average channel widths (n=5 devices per data point) are plotted against the size of the corresponding channel in the mask parts. Error bars show the standard deviation.
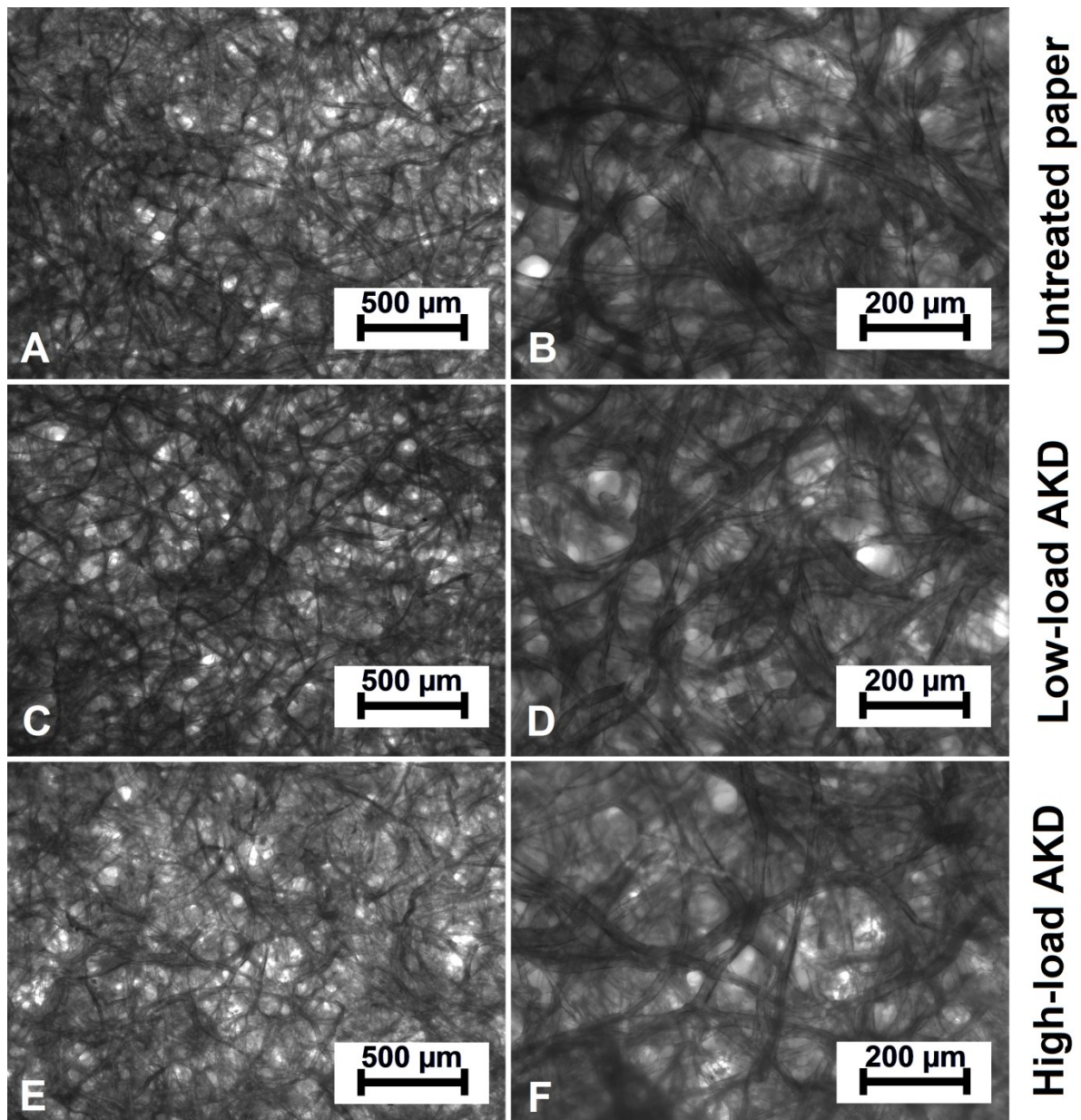
Figure S-2: Microscopic images of (A, B) untreated cellulose paper, (C, D) a low-load AKD region and (E, F) a high-load AKD region with (A, C, E) a 4x objective and (B, D, F) a 10x objective. These images show that there is no clear deposition of AKD in between the cellulose fibers of the porous network. This again means that the hydrophobicity of the paper is altered by changes in the surface energy of the fibers, as expected, rather than by physical obstruction of flows.
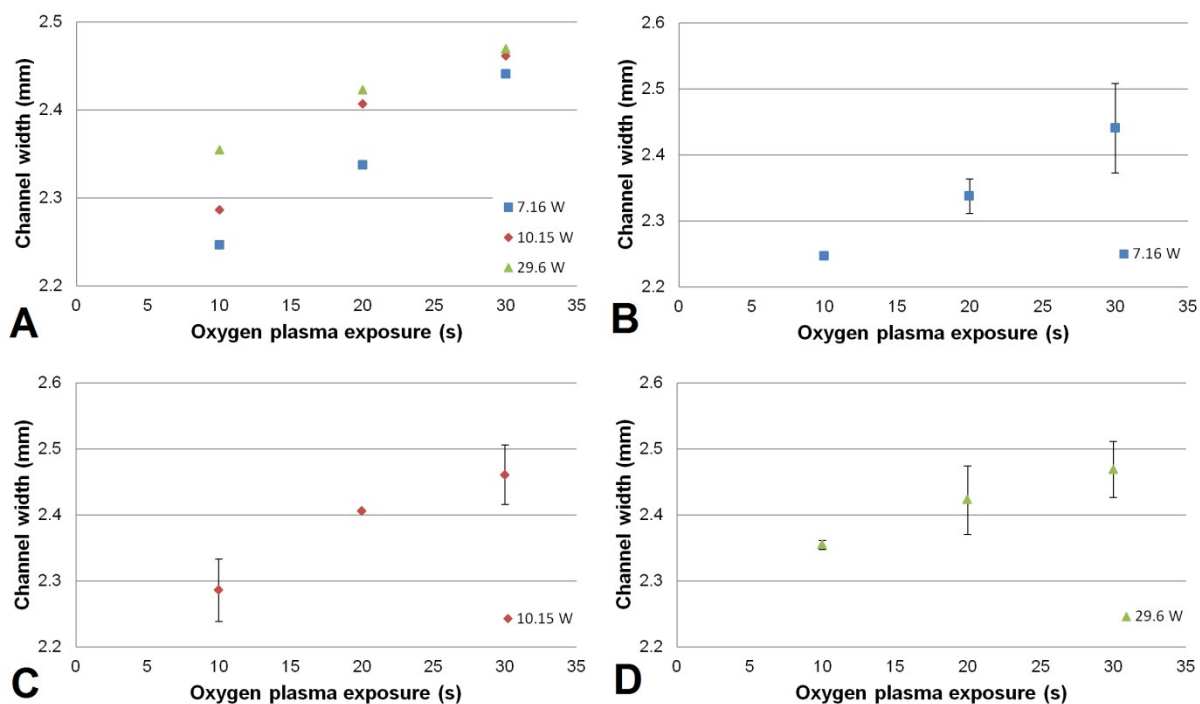
Figure S-3: The influence of oxygen plasma exposure time and power on channel width for the first AKD patterning step (0.6 g/L AKD in hexane). The mask parts were designed to have a 2-mm-wide channel. The actual channel width in the mask was 1.8 mm. Exposure times were varied from 10 to 30 seconds. The different power settings were (B) 7.16 W, (C) 10.15 W, and (D) 29.6 W. Error bars show the standard deviation. All data points are averaged (n=3 devices), except for the 10 s exposure on 7.16 W. This condition was measured only once, because the hydrophilization was so poor that it was difficult or impossible to wet the channel structures and thus perform the measurement.
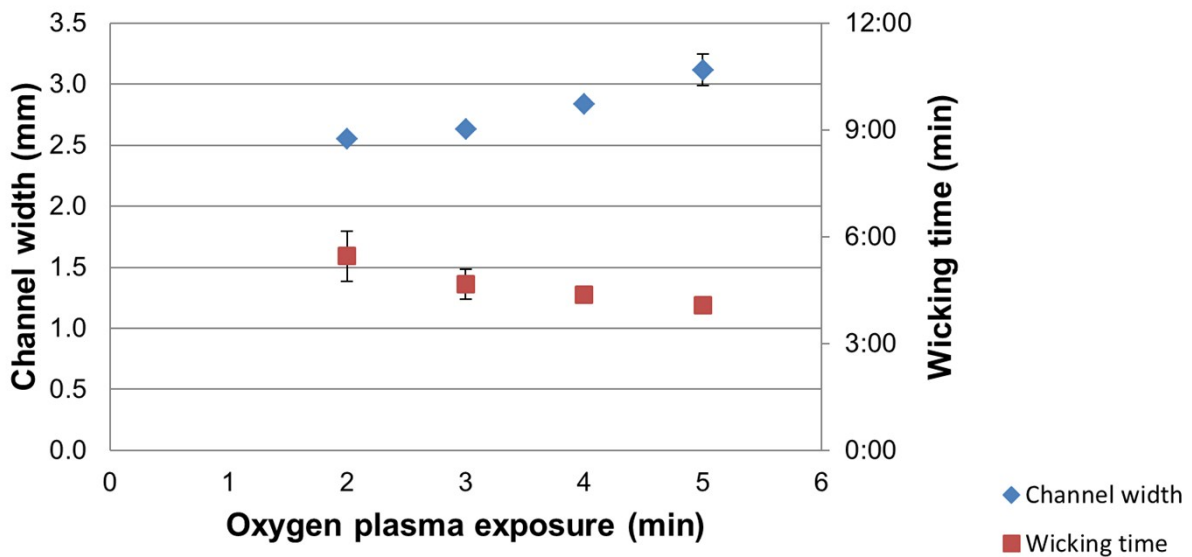
Figure S-4: The influence of oxygen plasma exposure on channel width and hydrophilicity of the channel after a single AKD patterning step with an increased AKD concentration (5.0 g/L in hexane). Hydrophilicity of the channel structure was quantified indirectly by checking how much time it took for water to run through the entire channel (wicking time). The averages of the channel width and the wicking time (n=3 devices per data point) are plotted against the duration of the oxygen plasma exposure. The mask parts were designed to have a 2-mm-wide channel. The actual channel width in the mask was 1.8 mm.
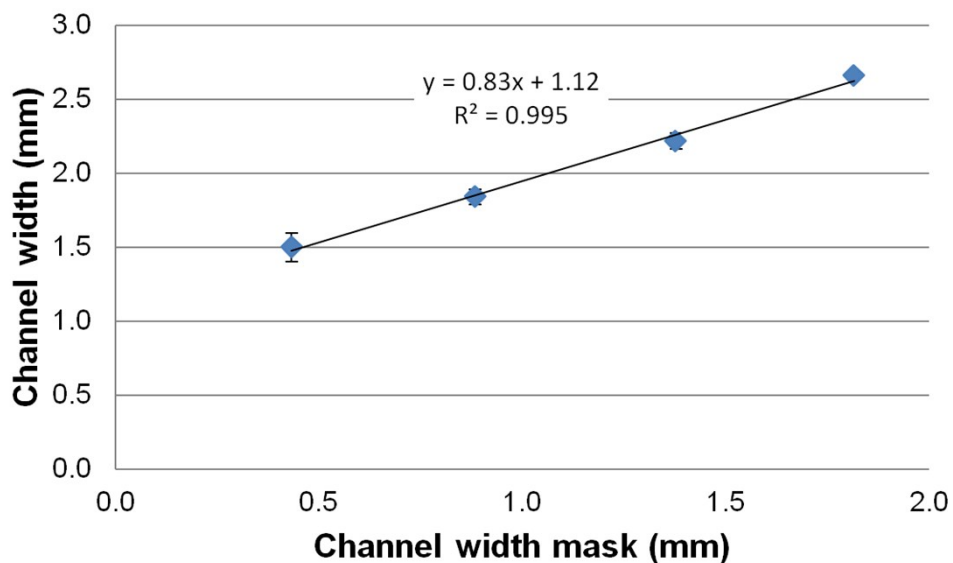
Figure S-5: Characterization of the paper patterns with water after a single AKD patterning step, with an increased AKD concentration (5.0 g/L in hexane). The paper samples were exposed to oxygen plasma for 3 min at 29.6 W. The average channel widths (n=5 devices per data point) are plotted against the size of the corresponding channel in the mask parts. Error bars show the standard deviation.
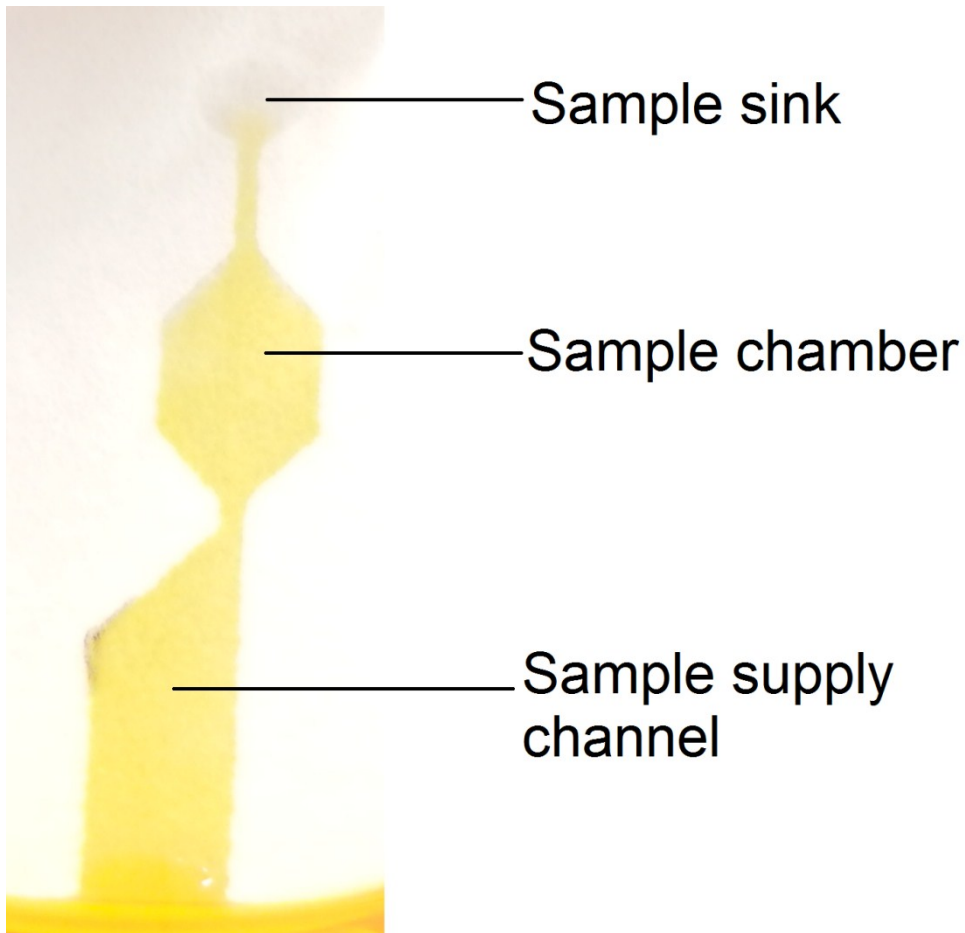
Figure S-6: Demonstration of the sample sink. Sample can be loaded into the device via the supply channel. As the sample fills up the channel and the sample chamber, retention of analytes on the paper will occur. This means that the fluid front mainly consists of solvent (*i.e.* water), and thus does not properly represent the sample. A sample sink is integrated into this design. The 'diluted' sample at the fluid front will leave the sample chamber into this sample sink, which can clearly be seen in this figure. The contents of the sample chamber, which will be eluted perpendicularly at a later stage, are no longer diluted and thus will better represent the actual sample.
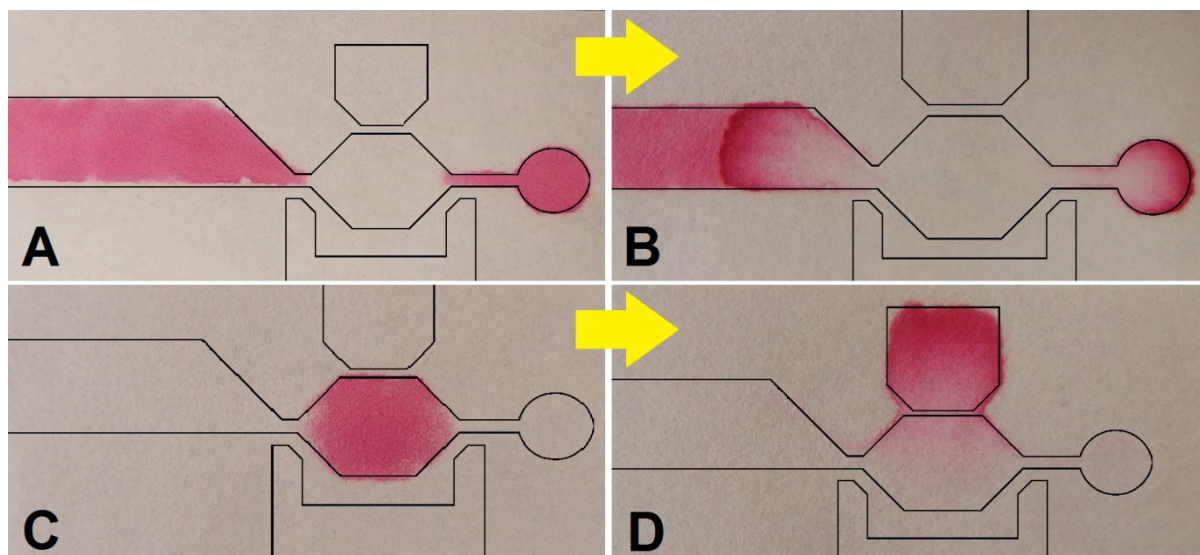
Figure S-7: Demonstration of the sampling efficiency of the volume-defined sampling device. The layout of the device is drawn in each photograph to clarify which regions of the device are being discussed. Red dye solution is applied with a micropipette to either (A) the sample supply channel plus the sample sink, or to (C) the sample chamber. After drying, both devices were eluted perpendicularly with 55% ethanol in water. Figures B and D show the devices after elution and drying. Volume-defined sampling means that the contents of the chamber should be eluted upwards into the collection chamber, whereas the contents of the channel and the sink should not. B and D illustrate that this goal is actually achieved with the paper device.
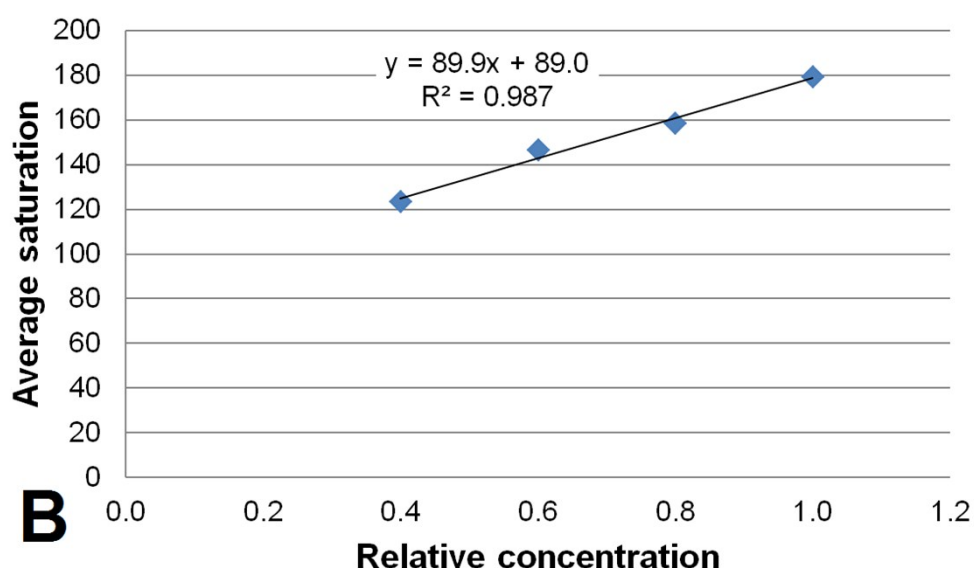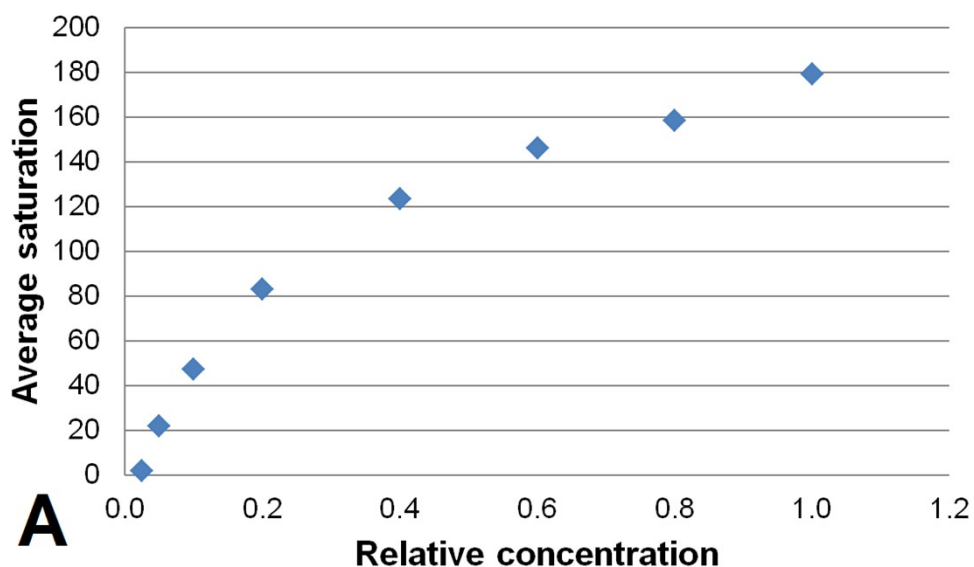
Figure S-8: Concentration dependence of saturation values from the *hue, saturation, brightness* (HSB) color space. A yellow dye solution (E102, E124) in water was prepared to yield a dark yellow color. As the concentration of the concentrated dye solution was unknown, this solution was arbitrarily assigned the dimensionless concentration '1'. This solution was then diluted, and each dilution was given a relative concentration based on this first solution. 3 µL of each solution was spotted on a piece of chromatography paper. The dried paper was scanned from both sides and analyzed with ImageJ in the HSB display. (A) The average saturation is plotted against the relative concentration. (B) Linear dependence on concentration was found in the saturation range of approximately 120-180 (maximum value for saturation in ImageJ is 255).
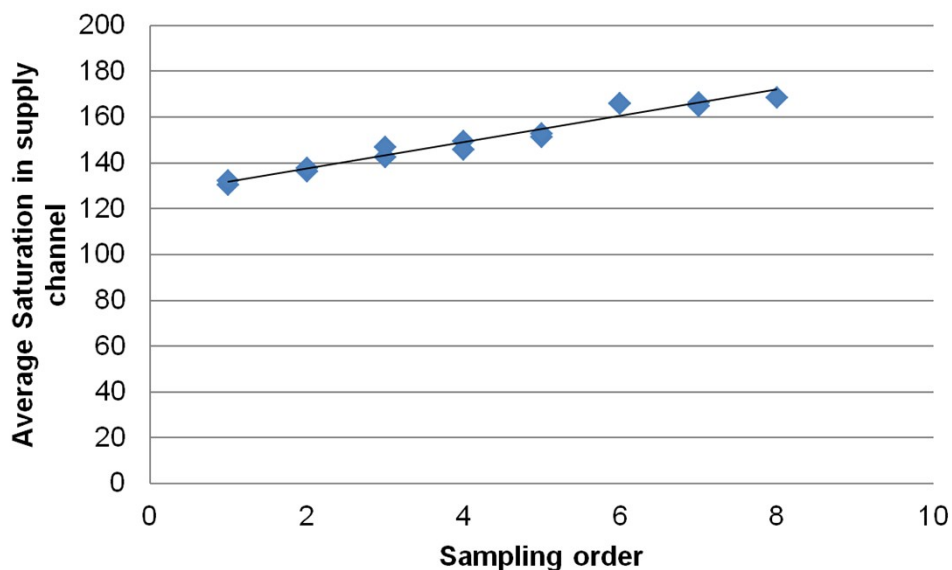
Figure S-9: Evaporation effect during sampling. The paper devices which were fabricated to demonstrate volume-defined sampling were used to sample a yellow dye solution. This sample solution was poured onto a watch glass, and one or two devices at a time were dipped into this solution until all devices had been used. After drying, the devices were scanned from both sides and the scans were opened in HSB display in ImageJ. The average saturation was measured in the center of the sample supply channel for each device by analyzing an area of approximately 3 x 3 mm. These values were plotted against the order in which the samples were taken. The graph clearly shows that the average saturation (which can be related back to concentration of the sample solution, Figure S-7) increases as samples were taken. This result indicates that the sample concentration was increasing over time, due to solvent evaporation during the sampling process. This influences the data, and thus should be corrected for. The devices were used for sampling in the following order (described by the respective value of X for the device and whether it was the first, second or third device of that X-value to be used): *(1) 1.40 (i), 1.75 (i); (2) 2.07 (i), 2.36 (i); (3) 2.64 (i), 2.64 (ii); (4) 2.36 (ii), 2.07 (ii); (5) 1.75 (ii), 1.40 (ii); (6) 2.64 (iii), 2.36 (iii); (7) 2.07 (iii), 1.75 (iii); (8) 1.40 (iii).*
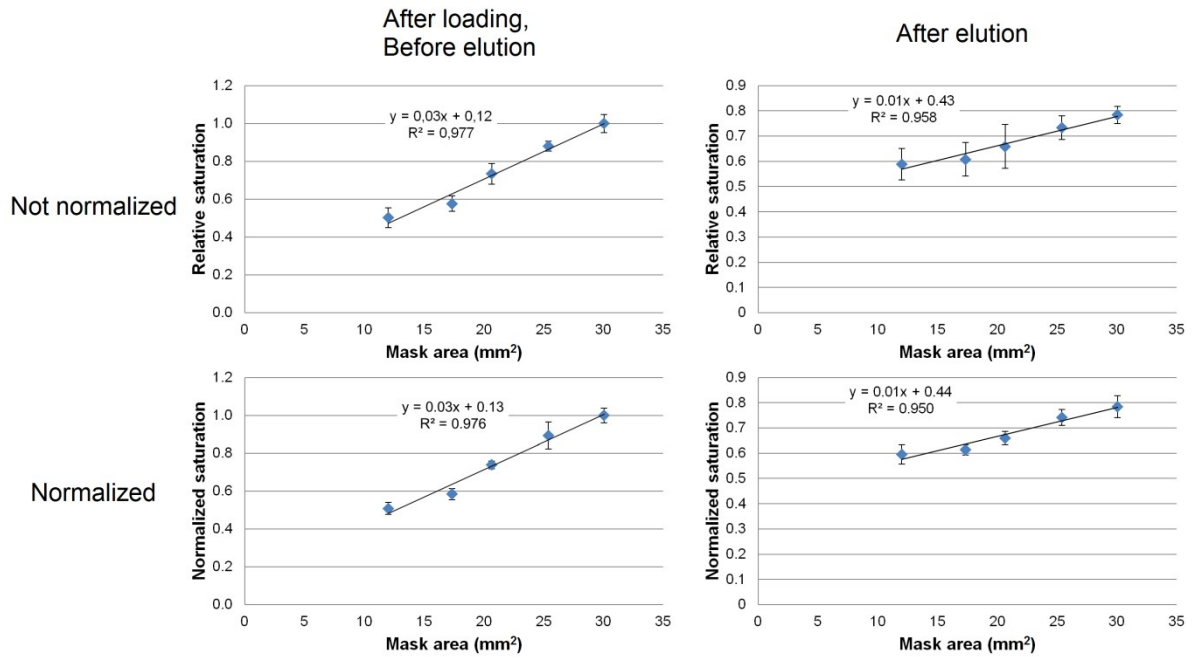
Figure S-10: Effect of normalization based on average saturation in the sample supply channel after sampling, but before elution. The average saturation was measured in the center of the supply channel, by selecting an area of approximately 3 by 3 mm. These graphs demonstrate that neither the distribution of the data points, nor the linearity are dramatically influenced by the normalization based on the average saturation. However, the variation in the results is much smaller after normalization.